# Sub-optimal Discontinuous Current-Clamp switching rates lead to deceptive mouse neuronal firing

**Marin Manuel**[1]

[1]**Université de Paris, SPPIN - Saints-Pères Paris Institute for the Neurosciences, CNRS, Paris, France**

**Abstract** Intracellular recordings using sharp microelectrodes often rely on a technique called Discontinuous Current-Clamp to accurately record the membrane potential while injecting current through the same microelectrode. It is well known that a poor choice of DCC switching rate can lead to under- or over-estimation of the cell potential, however, its effect on the cell firing is rarely discussed. Here, we show that sub-optimal switching rates lead to an overestimation of the cell excitability. We performed intracellular recordings of mouse spinal motoneurons, and recorded their firing in response to pulses and ramps of current in bridge and DCC mode at various switching rates. We demonstrate that using an incorrect (too low) DCC frequency lead not only to an overestimation of the cell conductance, but also, paradoxically, to an artificial overestimation the firing of these cells: neurons fire at lower current, and at higher frequencies than at higher DCC rates, or than the same neuron recorded in Bridge mode. These effects are dependent on the membrane time constant of the recorded cell, and special care needs to be taken in large cells with very short time constants. Our work highlights the importance of choosing an appropriate DCC switching rate to obtain not only accurate membrane potential readings, but also accurate representation of the firing of the cell.

## Keywords

Electrophysiology, Technique, DCC, intracellular recording, sharp micro-electrodes, neuronal excitability, firing frequency

# 1 Introduction

Neurons, by virtue of their plasma membrane and the numerous ion channels that can be found therein, behave—to a first approximation— like RC circuits. Consequently, a stationary electrical (ionic) current flowing through the membrane causes a change of voltage proportional to the resistance of the cell. This is Ohm's law: $V = I \times R$, where V is sometimes called voltage drop or IR drop. When performing intracellular recordings with microelectrodes, or whole cell recordings using patch electrodes, electrophysiologists can control the current flowing through their electrode ("current clamp") to change the membrane potential of the cell and thereby study its excitability. However, the electrode itself, because of its very small tip, acts as an additional RC circuit, and therefore also experiences an IR drop when current is applied. In these conditions, it is essential to be able to separate the physiological response of the cell from a change of voltage caused by the resistance of the very electrode used to perform the recording. Two main techniques have been developed over the years to overcome this problem. The first one, the so-called "bridge" mode, consists (broadly speaking) in subtracting the voltage drop caused by the current injection through a variable resistor set to a value close to the estimated electrode resistance from the voltage measured by the electrode. This technique works well if the resistance of the electrode can be assumed to be constant over a large range of current intensity. Unfortunately, that is often not the case, particularly with small intracellular microelectrodes, which can exhibit strong non-linearities. A second technique was invented in the early 1970s, which consists in injecting current and measuring the potential at separate times, hence the name "discontinuous current clamp" (DCC) (Brennecke and Lindemann, 1971; Finkel and Redman, 1984). Instead of injecting a continuous current, the amplifier will alternate at a high frequency between injecting a pulse of current (scaled appropriately so as to conserve the same charge transfer) for a very short duration (classically

1/3 of the DCC period), while no current is injected for the remainder of the DCC period. The membrane potential is sampled at the end of the period, when no current is injected through the microelectrode. If the time constant of the electrode is fast enough compared to the time constant of the membrane, then the IR drop through the electrode has had time to vanish when the potential is sampled, while the IR drop through the membrane would have barely decayed. In theory, these two recording modes (bridge and DCC) should yield the same values of membrane potential, as long as they are used in the proper conditions. One important aspect parameter is the DCC switching rate, which needs to be high enough so that the membrane time constant can smooth out the short pulses of current, but not so high as to prevent the IR drop through the electrode to vanish before the end of the sampling period. An incorrectly set DCC rate should, in theory, only lead to under- or over-estimating the membrane potential. Yet, a recent study (Jensen et al., 2020) illustrates that the firing behaviour of a spinal motoneuron in response to a triangular ramp of current can change drastically depending on the DCC switching rate set by the experimenters, suggesting that the choice of the DCC switching rate is a critical parameter to take into consideration not only in order to obtain accurate readings of the membrane potential, but also when studying the firing rates of the cell. In this paper, We demonstrate that using a sub-optimal (too low) DCC frequency lead not only to an overestimation of the cell conductance, but also, paradoxically, to an artificial overestimation the firing of these cells: neurons fire at lower current, and at higher frequencies than at higher DCC rates, or than the same neuron recorded in Bridge mode.

## 2 Results

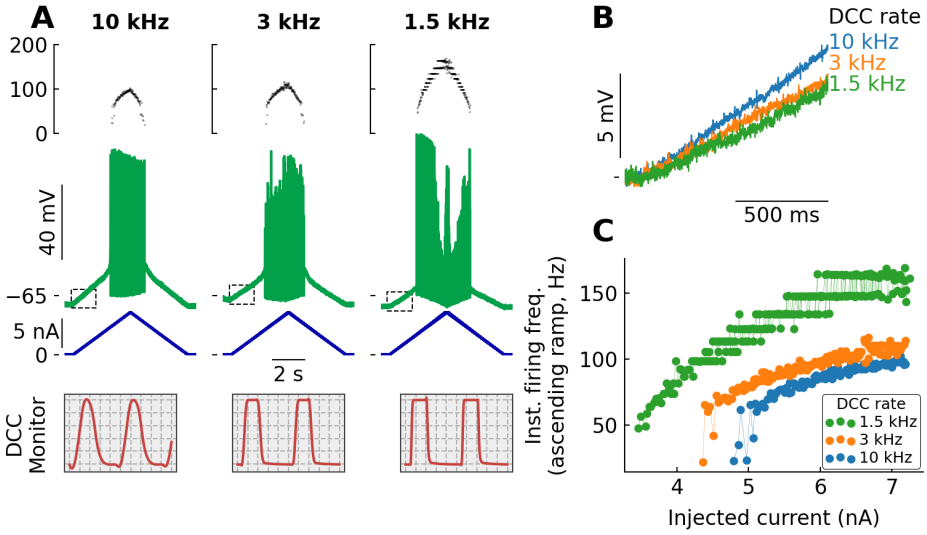


**Figure 1. Typical example showing how DCC rates alter the response of a motoneuron to a stationary input.** **A.** Response of a triceps Surae motoneuron ($R_{in}$=3.8 MΩ; $\tau_m$=3.3 ms) to a slow (1 nA/s) triangular ramp of current, recorded in DCC mode with switching rates 10, 3 and 1.5 kHz. Bottom traces: injected current. Middle traces: voltage response. Top traces: instantaneous firing frequency. The boxes on the bottom represent the monitoring traces used to check the settling of the electrode, recorded at the top of the ramp. Time bases from left to right: 20 μs, 67 μs, and 133 μs per division. **B.** Expansions of the regions delimited with the dashed box in A. **C.** F-I curves showing the instantaneous firing frequency plotted against the injected current at the time of each spike.

## 2.1 Case study

Let us start by observing the effect of changing the DCC rate on the response of a motoneuron to a triangular ramp of current. When recorded with a DCC rate of 10 kHz, the motoneuron depolarized progressively until it started to fire repetitively (Figure 1A). The initial firing was irregular and accelerated very steeply over the first few spikes. Then, the firing became more regular and increased approximately linearly with the injected current (Figure 1C). This is the classical response of mouse spinal motoneurons to this kind of current injected: a brief sub-primary range, followed by a linear primary range (Manuel et al., 2009; Iglesias et al., 2011). When recorded with a DCC rate of 3 kHz, the response was similar, but quantitative differences were visible. First, the rate of rise of the membrane potential before the onset of firing was slower than at 10 kHz (Figure 1B). Since the current increases linearly,

the rate of rise of the membrane potential is directly proportional to the resistance of the cell. At 3 kHz, the cell thus appears to have a higher conductance than at 10 kHz. Paradoxically, even though the conductance was seemingly increased, the cell started firing at a lower current intensity, and at higher frequencies than at 10 kHz (Figure 1C). These effects were even more pronounced at lower DCC rates. At 1.5 kHz, the apparent conductance was larger than at 10 and 3 kHz (lower rate of rise of the potential, Figure 1B) and the firing started even sooner (Figure 1C). In addition, at 1.5 kHz, the firing frequency increased very steeply with the injected current and reached much higher values ($>$ 100 Hz) than with higher DCC rates. Moreover, when the firing frequency increased beyond 100 Hz, the firing acquired a very distinctive step-like pattern, where the firing frequency had a tendency to oscillate back and forth between two discrete values (Figure 1C).

## 2.2 DCC switching rate affects the apparent cell conductance

The first effect outlined above, namely the increase in cell conductance at low DCC rate, is fairly straightforward to explain. By design, in DCC mode, the amplifier injects a short pulse of current, then stops the injection to allow the voltage drop through the electrode to vanish before the membrane potential is sampled. However, during that time of no current injection, the membrane potential will also decay. The technique only works if the electrode time constant (adjusted to be as fast as possible using the capacitance compensation circuit of the amplifier) is much faster than the membrane time constant. In these conditions, the DCC frequency can be set high enough that the membrane potential has barely decayed by the time the voltage is sampled, and the membrane potential recorded in DCC mode is very close to the membrane potential that would be recorded with a perfectly balanced bridge (Figure 2B). If the DCC rate is too low, however, then the membrane potential has time to decay in between the end of the current pulse and the sampling time (Figure 2A). Consequently, the membrane potential recorded in DCC mode is lower

than it would be when recorded in bridge mode. Since the current intensity applied by the amplifier is the same in all cases, an underestimation of the membrane potential produces an apparent increase of the cell conductance at low DCC rates. Conversely, if the DCC rate is too high, then the IR drop through the electrode does not have time to vanish by the time the potential is sampled (Figure 2C). Therefore the value of the membrane potential of the cell is contaminated by a fraction of the IR drop through the electrode, leading to an overestimate of the potential, and thus an apparent decrease in cell conductance (Figure 2C).

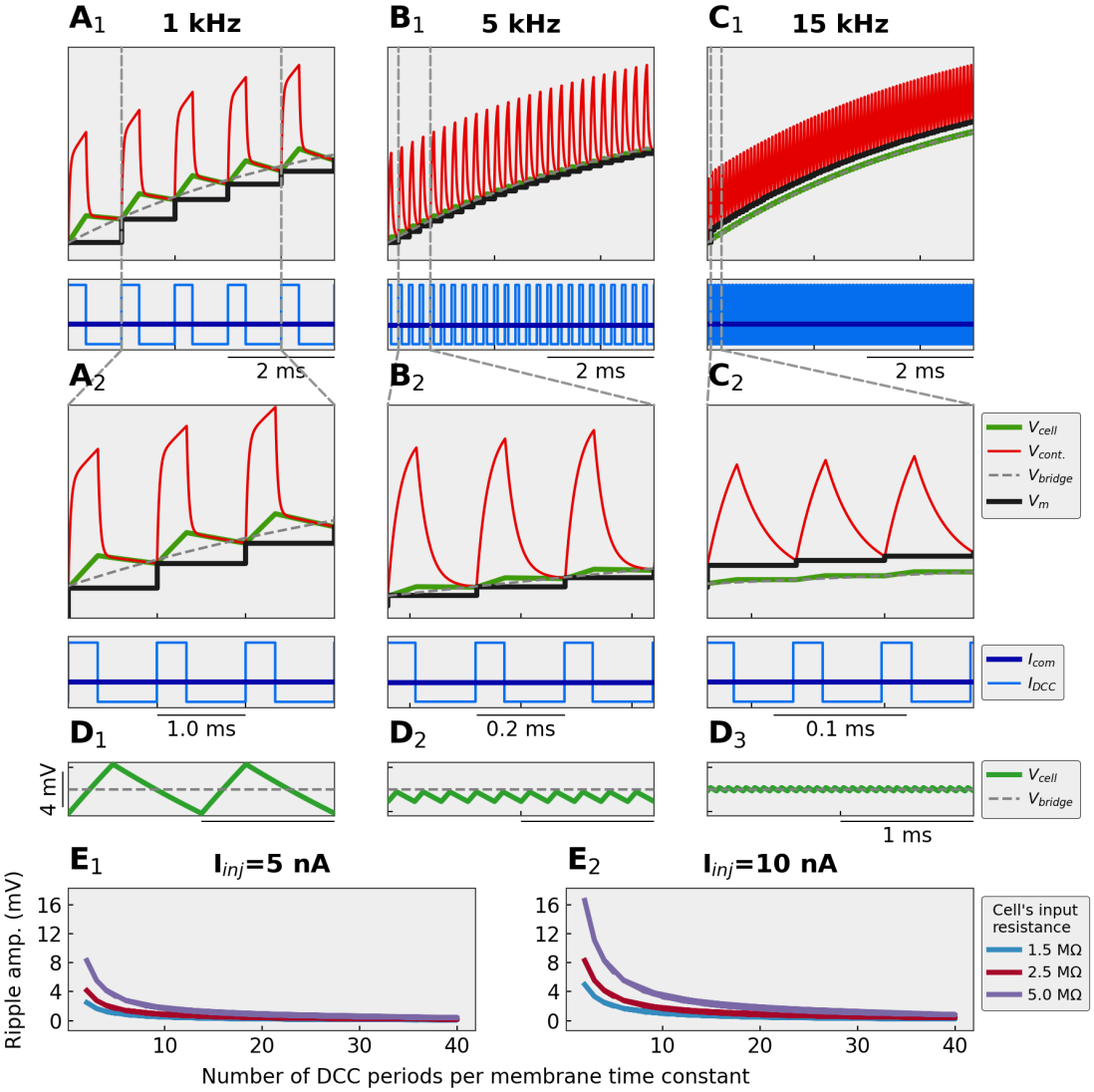

**Figure 2 *(previous page).* Effect of DCC rate on the recording of the membrane potential.** Numerical simulations showing the response of a neuron to a square pulse of current. The simulated cell had a resistance of 5 MΩ and a time constant of 5 ms. The electrode had a resistance of 1 MΩ and an effective time constant 200× faster than the membrane time constant. **A.** recording with a DCC rate of 1 kHz (5 cycles per time constant). The arrowheads point to sharp oscillations in the membrane potential. **B.** recording with a DCC rate of 5 kHz (25 cycles per time constant). **C.** recording with a DCC rate of 15 kHz (75 cycles per time constant). **D.** Traces showing the steady-state amplitude of the membrane potential ripples in a cell with an input resistance of 2.5 MΩ, time constant 3 ms, and injected current 10 nA when recorded in DCC mode at 1 kHz ($D_1$), 5 kHz ($D_2$), and 15 kHz ($D_3$). **E.** Plots showing the amplitude of the ripples as a function of the normalized DCC frequency (number of DCC cycles per membrane time constant). The response was measured in steady-state for two current intensities that are routinely reached during our recordings in mouse spinal motoneurons (5 nA $E_1$, and 10 nA $E_2$) and for three values of the cell's input resistance (which correspond to typical values for FF 1.5 MΩ, FR 2.5 MΩ, and S motoneurons 5 MΩ). $V_{bridge}$: response of the cells to the continuous current as would be observed in an ideal situation where the electrode resistance was perfectly compensated for by the bridge circuit. $V_{cont.}$: continuous voltage recorded at the tip of the electrode that includes the voltage drop through the electrode and the cell membrane. $V_m$: output of the amplifier, which is the value of $V_{cont.}$ sampled at the end of each DCC period (diamonds) and stored in a sample-and-hold circuit. $V_{cell}$: calculated membrane potential excluding the contribution of the electrode resistance. $I_{com}$: stationary current that the experimenter is imposing to the cell. $I_{DCC}$: actual current injected in the cell. That current is 3× the amplitude of $I_{com}$, but injected for only 1/3 of the time.

## 2.3 Low DCC switching rates can drive firing

The effect of the DCC on the F-I curves is more subtle. Although the amount of charge transferred to the cell is the same in DCC and in Bridge, the frequency content of the input is not the same. By chopping the current injection in short pulses, the DCC introduces harmonics of the DCC frequency in the input signal (Brette and Destexhe, 2012). This is particularly problematic at low DCC rates, where the membrane potential has time to increase during the pulse injection and then has time to decay substantially in between each current injection, creating "ripples" in the membrane potential (Finkel and Redman, 1984) (Figure 2). Note that although these ripples are present in the membrane potential, they are hidden to the experimenter by the DCC sample-and-hold circuit, which samples the potential at the end of the DCC period and holds the amplifier output constant at that value until the next sampling time. We therefore relied on numerical simulations to investigate these ripples. Figures $2D_{1–3}$ show examples of steady-state ripples experienced by a model of a typical FR motoneuron when injected with 10 nA of current in DCC mode at 1, 3, and 8 kHz. Because the actual current injected during the DCC pulses are 3× the intensity of the desired current, these ripples can be quite large. The amplitude of these ripples depends not only on the DCC frequency, but also on the time constant of the membrane (as well as, of course, the resistance of the cell and the intensity of the injected current). We therefore normalized the DCC rate by the membrane time constant (number of DCC periods per time constant). Figures $2E_{1–2}$ show how the amplitudes of the ripples change with DCC rate for three values of the motoneuron input resistance (1.5 MΩ, 2.5 MΩ, and 5 MΩ, corresponding to typical values for, respectively, FF, FR and S mouse motoneurons (Martínez-Silva et al., 2018)), and two values of injected current (5 and 10 nA, which are values that are typically reached when injecting ramps of current in mouse motoneurons). These figures show that the amplitudes of the ripples increase steeply when the DCC switching

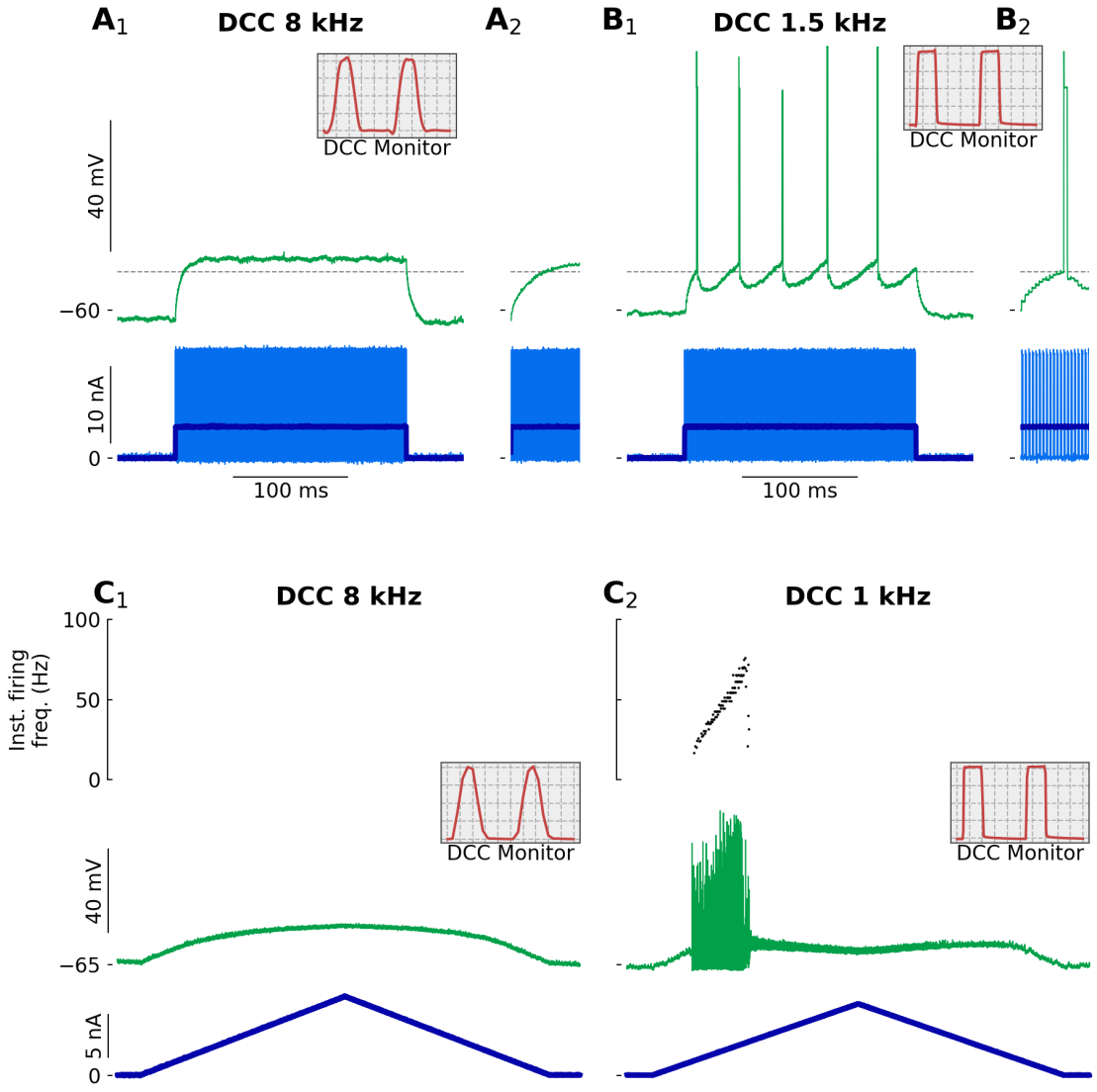


rate is decreased, particularly under 10 DCC periods per time constant. However, even for reasonable rate (10–20 DCC periods per time constant), the ripples can reach several millivolts in amplitude.

As discussed above, using a low DCC frequency becomes equivalent to injecting a series of short pulses of current. This kind of stimulus is highly efficient to trigger motoneuron firing, much more than a continuous current injection (Delestrée et al., 2014; Martínez-Silva et al., 2018). Figure 3A shows the response of a motoneuron to the same 200 ms-long 4 nA pulse of current, recorded in DCC mode with a rate of

**Figure 3 *(previous page).*** **Spurious firing elicited by low DCC rates. A–B.** Recording from a Triceps Surae motoneuron ($R_{in}$=3.5 MΩ; $\tau_m$=4.9 ms) following the injection of a 200 ms-long 4 nA pulse of current. A. Response recorded with a DCC rate of 8 kHz. The inset in A2 is a zoom over the first 15 ms following the onset of the pulse. B. Response recorded with a DCC rate of 1.5 kHz. The inset in B2 is a zoom over the first 15 ms following the onset of the pulse. The horizontal dashed line represents the voltage threshold measured at the foot of the first spike of the response in B. The grey boxes in A and B represent the monitoring traces used to check the settling of the electrode, recorded at the top of the ramp. Time bases from left to right: 25 μs ($C_1$), and 133 μs ($C_2$) per division. **C.** Response of a Triceps Surae motoneuron ($R_{in}$=5.0 MΩ; $\tau_m$=4.7 ms) to the injection of a triangular ramp of current (1 nA/s) with a DCC rate of 8 kHz ($C_1$) or 1 kHz ($C_2$). The bottom trace is the injected current, the middle trace is the membrane potential and the top graph is the instantaneous firing frequency. The inserts represent the monitoring traces used to check the settling of the electrode, recorded at the top of the ramp. Time bases from left to right: 25 μs (C1), and 200 μs (C2) per division.

1.5 kHz and 8 kHz. With a DCC at 8 kHz, this pulse of current was not able to reach firing threshold (Figure $3A_1$). At lower DCC rate, however, although the amount of current injected is the same, the motoneuron responded with a strong repetitive discharge (Figure $3B_1$). Interestingly, the voltage threshold for the first spike was below the steady-stage potential reached with a DCC of 8 kHz (compare dashed lines in Figure $3A_2$ and $B_2$), suggesting that the appearance of firing at 1.5 kHz was not due to a larger depolarisation (in fact, the depolarisation is smaller, see above), but rather due to the strong sensibility of the cell to transient currents and ripples in their membrane potential. In the extreme case, a low DCC rate can turn a motoneuron that was not able to fire repetitively in response to a stationary input (Figure $3C_1$) into a motoneuron that elicits a bout of repetitive firing to the same ramp (Figure $3C_2$). Observation of the DCC monitoring trace on the oscilloscope (inserts in Figure 3C) confirms that the inability to fire repetitively was not due to the electrode becoming blocked. The IR drop through the electrode had fully vanished by the end of the DCC period, and the membrane potential was therefore accurately measured. With a DCC at 1 kHz, however, the DCC period was so long that not only the IR drop through the electrode had time to settle to zero, the membrane potential also rose and decayed during each DCC period. The net effect is a series

of large amplitude membrane potential ripples (which are hidden by the sample-and-hold circuit of the amplifier), superimposed to the slow depolarization of the quasi-stationary ramp. The spiking observed in these conditions is caused by this mixed dynamic and stationary input, rather than a response to the stationary input alone.

As hinted above (Figure 1), this effect can profoundly affect the shape of the frequency-current relationship of a motoneuron in response to a triangular ramp of current, but which F-I curve is the most physiological? Figure 4 illustrates the response of a motoneuron to a series of ramps of current recorded in DCC mode at various frequencies. Because this motoneuron had a fairly low rheobase and did not require a lot of current to fire, we were able to record the response in Bridge mode as well. That response is free of artefacts due to DCC switching, and we will therefore use it as the control firing for this cell. As can be seen, the response recorded in DCC mode at 8 kHz is almost indistinguishable from the one recorded in Bridge mode (Figure 4B). However, when the DCC frequency is too low, the curve is shifted to the left (lower recruitment current), the slope is steeper, and a distinctive “step” pattern appears on the instantaneous frequency.

This effect is seen consistently across motoneurons. Figure 5A–D shows how the current intensity required to start firing (onset current), the current intensity when the cell stopped firing (offset current), the slope of the ascending phase of the F-I relationship (F-I gain), and the voltage threshold measured on the first spike of the ramp vary with DCC frequency. It is clearly apparent that values measured at low DCC rates are usually very different than the ones measured at higher rates, and that the values tend to converge to a stable value when the DCC rate is increased past a critical point. Moreover, in the motoneurons in which we were able to record the response in Bridge mode (Figure 4), the values measured with the highest DCC rates agree well with the values recorded in bridge mode (diamonds), with the exception of the voltage threshold, which cannot be measured accurately in bridge mode since

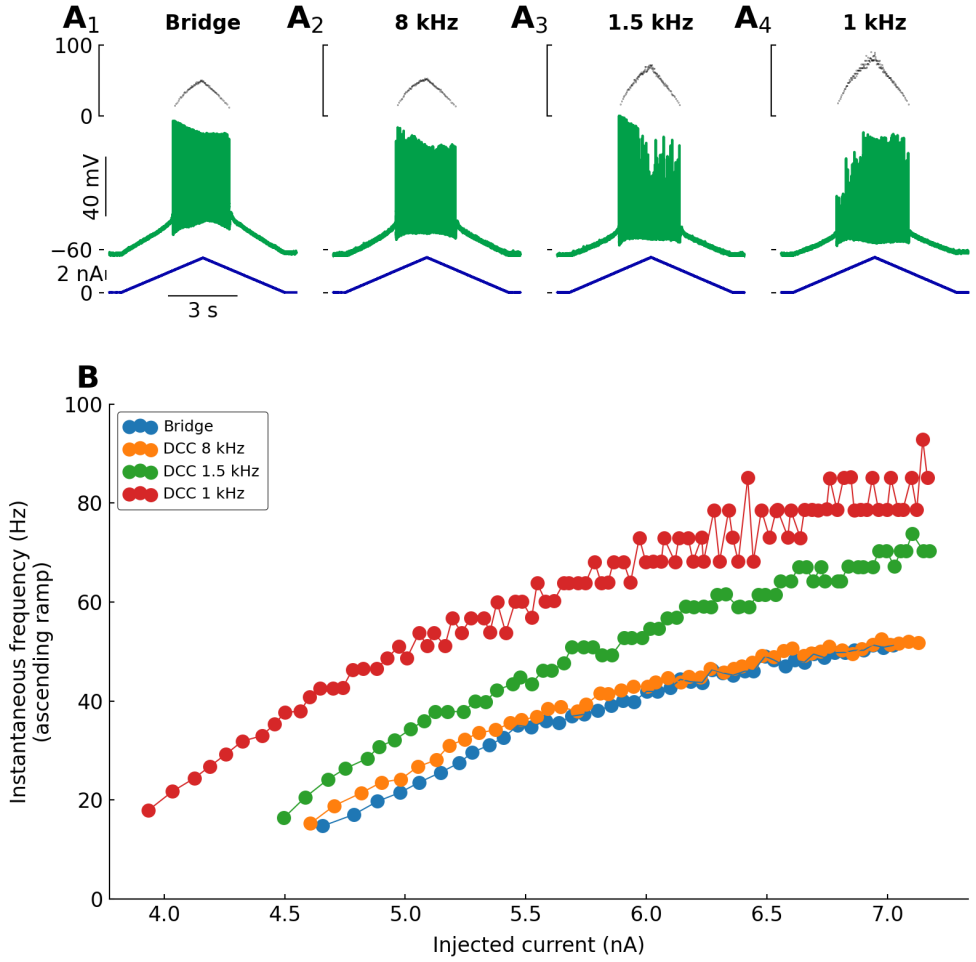


**Figure 4. Effect of DCC switching rate on the response to a ramp of current. A.** Same motoneuron as Figure 3A–B, injected with a triangular ramp of current (2 nA/s) and recorded either in Bridge mode ($A_1$), or in DCC mode at various switching rates ($A_2$: 8 kHz, $A_3$: 1.5 kHz, $A_4$:1 kHz). **B.** The instantaneous firing frequency on the ascending ramp is plotted against the current intensity.

one cannot completely get rid of the IR drop through the electrode in this mode. Because the effect of the DCC rate depends on the time constant of the cell, the plateau value is reached for different DCC rates in each motoneuron. We therefore normalized the DCC rate in each cell by the membrane time constant (number of DCC periods per time constant), and we normalized the measured value to the value estimated at the highest DCC rate (Figure 5E–F). These curves clearly show that all measurements converge towards the same value as the DCC switching rate is increased. However, these curves demonstrate that the rate of 10 cycles per time constant recommended in the Axoclamp manual is not high enough. Rates of at least 15–20 cycles per time constant are necessary to get good estimates of the value of most of these measurements.

## 2.4 Low DCC rates entrain firing at discrete intervals

As shown above, using a low DCC switching rate not only leads to cells firing at lower current, but also at higher frequencies. For instance, in the cell exemplified in Figure 6A, lowering the DCC rate from 8 to 3 kHz led to both a leftward and upward shift of the F-I curve. Reducing it further to 1 kHz led to the appearance of marked “plateaus” in the instantaneous firing frequency. This behavior can be reproduced in a simple integrate-and-fire model (Figure 6B). These plateaus correspond to interspike intervals (ISI) that are multiples of the DCC switching period. The cell no longer fires at its natural interspike interval, but instead is driven to fire on the crest of the membrane potential ripples when the after-hyperpolarization from the preceding spike has relaxed sufficiently for the membrane potential to come close to the voltage threshold (Figure 6C). Because a significant amount of current has to be injected in spinal motoneurons to reach firing threshold, the ripples can get quite large (Figure 2E), which is why they can entrain firing with shorter ISI (higher frequency) than what would be observed for the same current intensity in Bridge mode (Figure 6C).

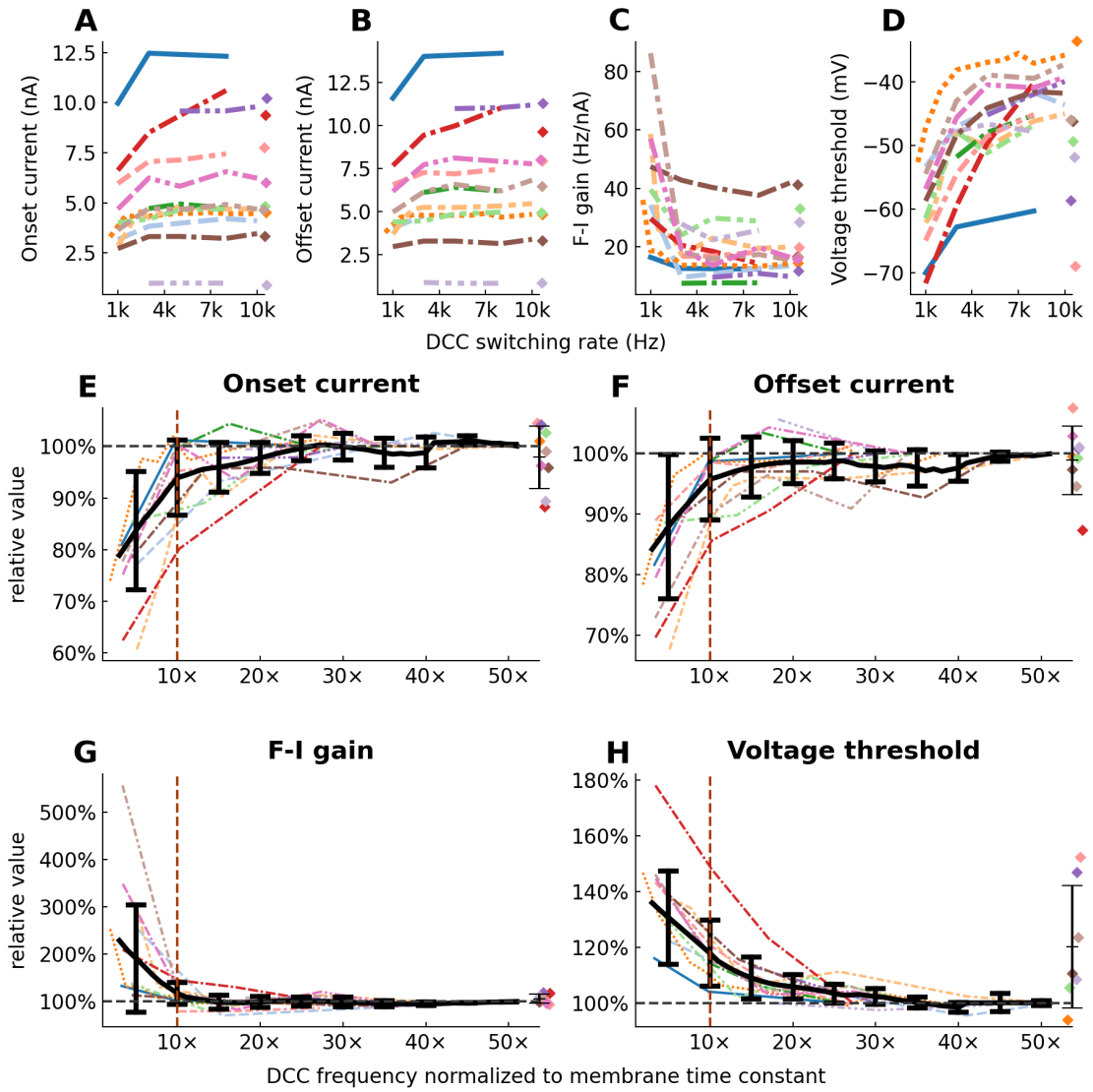


**Figure 5. Relationship between parameters measured on the F-I curves and the DCC frequency used during the recording.** In all panels, each line represents one motoneuron. The green dotted lines correspond to the motoneuron shown in Figure 4, and the parameters extracted from the trace recorded in bridge mode are represented by a green diamond on the right side of each plot. Onset current: current required to elicit the first spike on the ascending ramp. Offset current: current at which the firing stops on the descending ramp. F-I gain: slope of the F-I relationship measured on the ascending part of the ramp. Voltage threshold: voltage measured at the foot of the first spike elicited on the ascending ramp. **A–D.** Absolute value of each of the parameters plotted against the DCC rate used during the recording. **E–F.** Value of each of the parameters normalized to the value measured at the highest DCC rate achieved in each motoneuron (dashed horizontal line) plotted against the DCC rate normalized by the time constant of each motoneuron. The thick black trace represents the average values across motoneurons with error bars representing average±SD. The vertical dotted line shows the recommended minimal DCC rate of 10 cycles per membrane time constant.

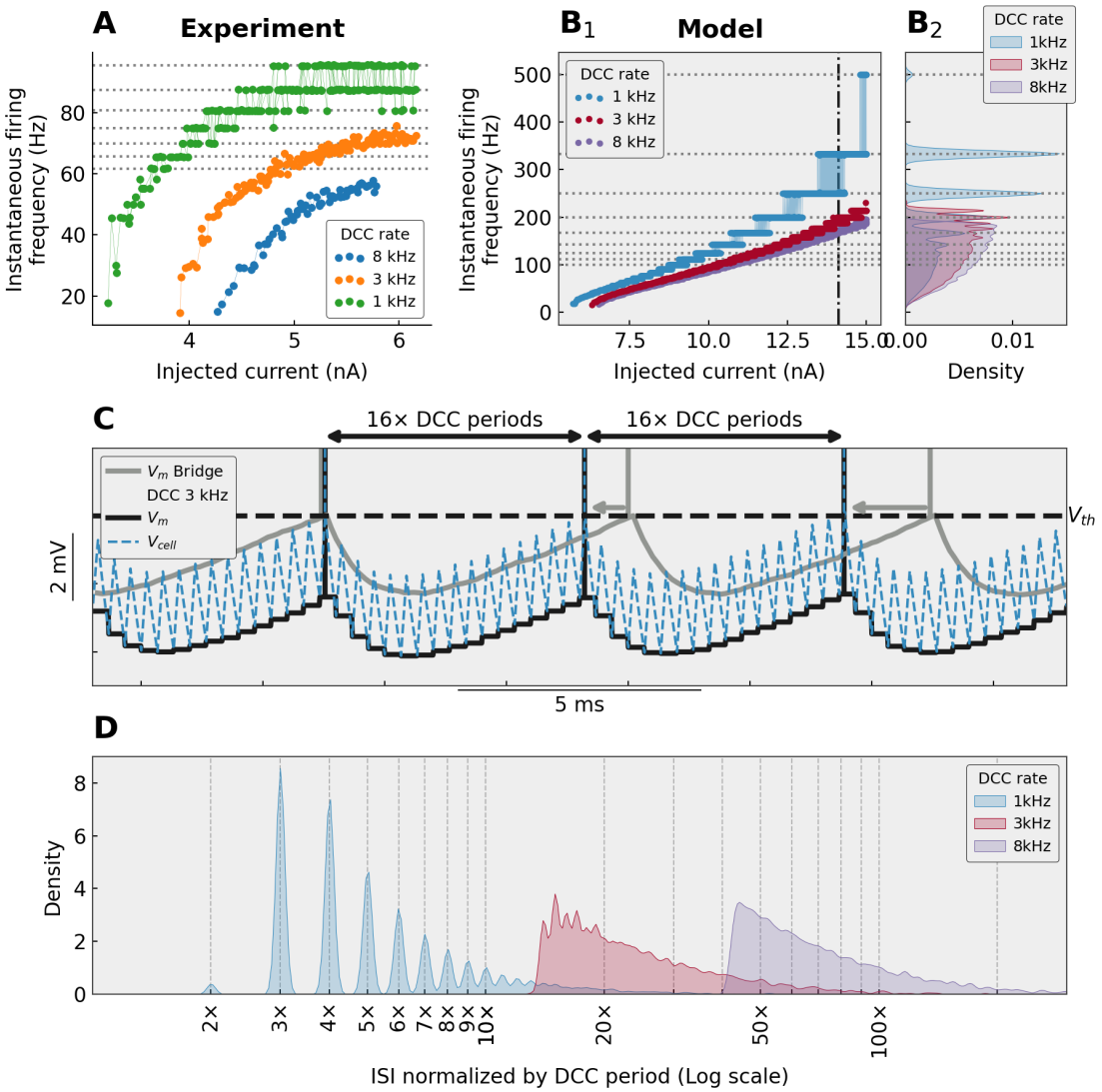

**Figure 6 *(previous page)*. Stepwise pattern is a sign of sub-optimal DCC rate A.** F-I curves from a Triceps Surae motoneuron ($R_{in}$=2.0 MΩ; $\tau_m$=3.8 ms), injected with a triangular ramp of current (1 nA/s) and recorded in DCC mode at three different DCC switching rates. At low DCC rates, a clear stepwise pattern is apparent, which corresponds to multiples of the switching rate (1050 Hz in this instance): 95.5 Hz (or 1 spike every 11 DCC periods), 87.5 Hz (1:12), 80.8 Hz (1:13), 75.0 Hz (1:14), 70.0 Hz (1:15), 65.6 Hz (1:16), etc. **B.** The same phenomenon can be observed in a simple integrate-and-fire motoneuron model. The model was that of a typical FF motoneuron ($R_{in}$=1.5 MΩ; $\tau_m$=2.0 ms), injected with a 10 nA slow ramp of current (1 nA/s), and recorded in DCC mode at 8, 3, and 1 kHz. A stepwise pattern is apparent at the top of the F-I curve at 3 kHz, and is clearly present at 1 kHz (see distinct peaks in the distributions of the firing frequencies in $B_2$). The horizontal dotted line represent the multiples of the period of the 1 kHz switching rates. The vertical dash-dotted line represent the region zoomed in in C. **C.** Comparison of the behavior of the model recorded in bridge mode (grey line) and in DCC at 3 kHz. The black line represent the $V_m$ output of the amplifier, while the dashed line represent the true membrane potential $V_{cell}$ which is hidden from the experimenter by the sample-and-hold circuit. The membrane potential ripples created by the DCC shorten the interspike intervals (grey arrows) and entrain the firing with interspike intervals that are multiples of the DCC period. **D.** Distribution of the interspike intervals obtained in DCC mode at 1, 3, and 8 kHz. The intervals have been normalized by the DCC period (1 ms, 0.33 ms, and 0.125 ms, respectively) and plotted on a logarithmic scale. At 1 kHz, the interspike intervals are concentrated at multiples of the DCC period.

The plateaus are characteristic of recordings with sub-optimal DCC rates for two reasons. Firstly, the amplitude of the ripples decreases with increasing DCC rates (Figure 2D), therefore they are less likely to "stick out" from the noise and entrain firing. Secondly, the plateaus are only apparent when the firing rate of the cell approaches the fundamental frequency of the DCC. Consider the behavior of the model in Figure 6B with a sub-optimal DCC frequency of 1 kHz (2 DCC cycles per membrane time constant). Firing starts at a low frequency then increases linearly without visible plateaus until the frequency reaches 50–60 Hz where they are barely visible but become much more prominent above 100 Hz. In this case, the plateaus appear when the firing is entrained at about one spike every 10 DCC cycles, and become more and more prominent as the firing frequency gets closer to the DCC rate: the distribution of the interspike intervals become more and more peaked at multiples of the DCC period (Figure 6D). Below 20 DCC cycles, even if entrainment happens, the difference between being entrained at one spike per e.g. 30 or 31 DCC cycles

is drowned in the variability of the discharge. Therefore, at higher DCC frequencies, not only do the ripples become smaller, but the range of firing frequencies over which plateaus are apparent is pushed higher and higher. For instance, in the model (Figure 6B), even though the firing frequencies largely overlap with DCC rates of 1, 3, and 8 kHz, firing rates reach one spike every 15 DCC cycles at 3 kHz (plateaus are clearly visible, Figures 6B$_{1-2}$,D), but barely reach one spike every 45 DCC cycles at 8 kHz (Figure 6D), and no plateaus are visible (Figure 6B).

Interestingly, this entrainment effect at sub-optimal DCC rates is able to induce an apparent increase in the slope in the F-I relationship, particularly when the firing frequency reaches high values. This phenomenon is illustrated Figure 7 where a motoneuron was stimulated with a high-amplitude (13 nA), fast ramp of current (5 nA/s), expressly for the purpose of pushing the motoneuron to high firing frequencies. At DCC rates 5 and 8 kHz, the resulting F-I curves are almost indistinguishable, with a first range of current where the frequency was increasing steeply, followed by a region where the frequency increased at a smaller rate (~7 Hz/nA, dashed grey line). When recorded with a DCC rate of 3 kHz, the F-I curve was shifted upward to higher firing frequencies. The slope of the initial linear phase was slightly higher (~10 Hz/nA, black dashed line) than with higher DCC rates. When the firing reached frequencies above 150 Hz, a clear step-wise pattern became apparent and the F-I curve became steeper (~20 Hz/nA), creating the illusion of a "secondary range", even though this change of slope is not present in the data recorded with higher DCC rates for the same current intensities. This effect is due to the fact that, when the DCC frequency is sub-optimal, ISI are entrained at multiple of the DCC period (Figure 6D). As the injected current and the frequency increases, the ISI shorten linearly by discrete steps (e.g. 1 spike every 10 DCC periods, then 1 spike every 9 DCC periods, then every 8 periods, etc...). Since the frequency is the inverse of the ISI, the firing frequency is increasing very steeply as it jumps from plateau to plateau (Figure 7B).

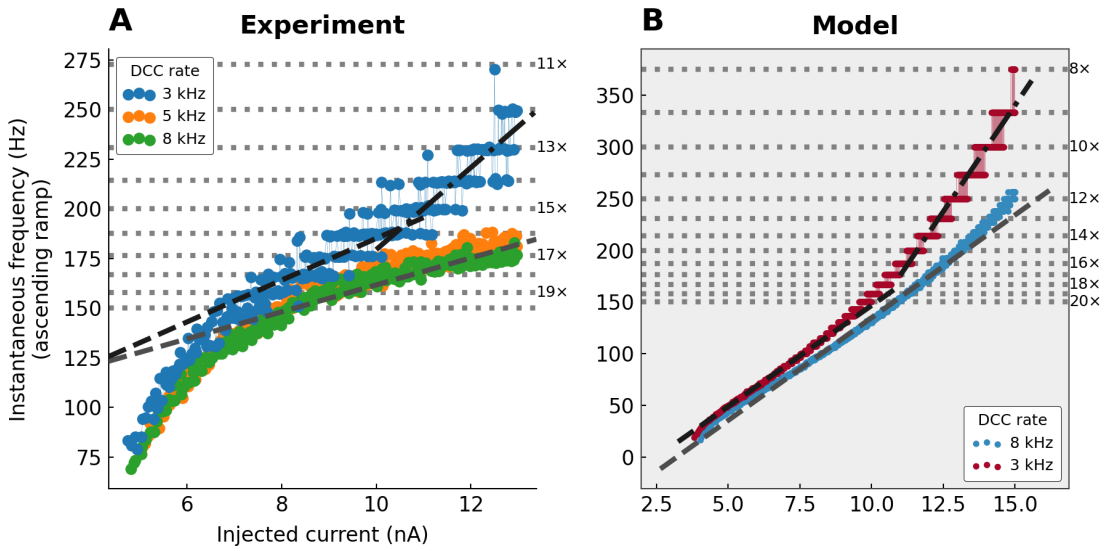


**Figure 7. Apparent change of slope in the F-I curve associated with discrete firing intervals. A.** F-I curves from a Triceps Surae motoneuron ($R_{in}$=4.1 MΩ; $\tau_m$=3.3 ms). A fast triangular ramp of current (amplitude 13 nA, 5 nA/s) was injected to drive the firing at high frequency. The instantaneous firing frequency is plotted against the ascending ramp current intensity. Grey dashed line: slope of the F-I curve recorded at 8 kHz measured in the second half of the curve. Black dashed line: slope of the F-I curve recorded at 3 kHz, measured over the range 7–10 nA. Black dash-dotted line: slope of the F-I curve recorded at 3 kHz, measured over the range 11–13 nA. Horizontal dotted lines: subharmonics of the 3 kHz DCC rate as indicated on the right of the plot. **B.** F-I curves obtained in a model with $R_{in}$=2.5 MΩ and $\tau_m$=2.0 ms. Compared to the F-I curve obtained with a high DCC rate of 8 kHz, which is mostly linear (grey dashed line), the F-I curve obtained with a DCC rate of 3 kHz clearly changes slope at ∼10 nA, from a slope roughly equal to the one measured at 8 kHz to a much steeper slope.

# 3 Discussion

This paper describes the effect of an incorrectly set DCC rate on the firing properties of spinal motoneurons. Although a low DCC rate lead to an underestimation of the membrane potential, and therefore an apparent increase in cell conductance, we show that, paradoxically, it has the potential to artificially drive the cells to fire a lower currents and higher frequency, as well as to profoundly alter the shape of the F-I relationship.

Although there are no theoretical upper limits to the DCC cycling rate, in practice, one is limited by the time constant of the electrode and the capacitance neutralization circuit of the amplifier. Indeed, if the voltage drop through the micro-electrode

has not relaxed to zero at the sampling time, the membrane potential recorded is contaminated by an unknown fraction of the electrode resistance. More importantly, there is a lower limit to the DCC rate. For instance, the Axoclamp manual states that the rate must be such that "that there are ten or more cycles per membrane time constant. This enables the membrane capacitance to smooth the membrane voltage response to the current pulses" (Axon Instruments, 2003). There must be a theoretical "optimal" DCC rate in between those two extremes, but finding that optimal frequency is difficult in practice (Brette and Destexhe, 2012). Instead, electrophysiologists observe the continuous electrode potential on an oscilloscope synchronized to the DCC sampling clock. The goal is to adjust the electrode capacitance compensation circuit and the DCC switching rate to reach the highest DCC rate possible while ensuring that the response shown on the oscilloscope appears flat, that is to say, that the contribution of the electrode resistance to the recorded potential has dropped down to zero before the time when the voltage is sampled.

While it is fairly straightforward to check that the DCC rate is not too high based on the settling time of the electrode observed on the monitoring oscilloscope, it is difficult to know whether the DCC rate is fast enough to not distort the firing of the cell. Our experiments show that the minimum value of ten cycles per time constant commonly recommended is too conservative. We show that DCC rates of at least 15–20 cycles per time constant are required to produce measurements that match the ones obtained in bridge mode. More importantly, above 15 cycles per time constants, the measurements become largely insensitive to the exact DCC rates, and therefore small differences in DCC rates (relative to the cell's membrane time constant) between cells should not impact their respective firing behavior.

Compared to the Bridge mode, the DCC transforms the input signal from a continuous variation in current intensity to a discontinuous situation, where the current can only be injected as short square pulses. This difference is almost negligible when the DCC rate is high enough for the membrane potential to barely move dur-

ing the current injection and the subsequent inter-pulse interval. However, at lower DCC frequencies, the membrane potential exhibit substantial ripples (Figure 2). It should be noted that, although these ripples are present across the membrane of the recorded cell, they are hidden from the experimenter since the output of the amplifier is held constant at the level of the previous sampled value during that time (thick black line in Figure 2A). When considering slow ramps of current, like in the present study, decreasing the DCC rate from a high frequency to a lower frequency therefore amounts to transitioning from a situation where the membrane potential is increasing slowly, to a situation where sharp voltage ripples are superimposed to a slow depolarisation. These ripples are particularly efficient at triggering action potentials, particularly when the membrane potential is very close to the firing threshold. Moreover, it has been shown in many neuronal types that the faster the rate of rise of the membrane potential, the more reliably a spike will be generated (Mainen and Sejnowski, 1995; Azouz and Gray, 2000; Agrawal et al., 2001; Kuo et al., 2006). This high dynamic sensitivity explains why motoneurons recorded with a low DCC rate fire at lower current despite reaching lower membrane potentials. In addition, it also accounts for the fact that, at low DCC rate, firing becomes entrained by the DCC. Membrane potential ripples trigger a spike more reliably than the slow decay of the after-hyperpolarization that follows the preceding spike. The interspike intervals thereby can only take values that are multiples of the DCC period, leading to the characteristic step-like pattern observed in the F-I curves.

Interestingly, motoneurons have a natural regime of firing where a similar step-like pattern can be observed in response to very slow current ramps. We have shown previously that, for a narrow range of current motoneurons exhibit subthreshold oscillations which alternate with spikes, producing a very irregular firing. This regime, called mixed-mode oscillations (MMOs) is responsible for the sub-primary firing range. These oscillations naturally emerge from a sodium to potassium ratio too weak to generate full blown spikes with high reliability; but when a spike is finally

generated, it is locked to one of the oscillations (Iglesias et al., 2011). However, since the frequency of the MMOs is much lower (100–125 Hz, Manuel et al., 2009; Iglesias et al., 2011), and disappear when the firing reaches past the transition frequency between the sub-primary and the primary range (Iglesias et al., 2011), the resulting plateaus in the F-I curve are only apparent over the sub-primary range.

As shown above, the distortions caused by the DCC rate are primarily dependent on the time constant of the membrane. In spinal motoneurons, there is a strong relationship between membrane time constant and cell size, such that small, Slow-type (S) motoneurons have a longer membrane time constant than the larger, fast fatigable (FF) motoneurons (Gustafsson and Pinter, 1984). Consequently, FF motoneurons require an even higher DCC frequency than S motoneurons to obtain accurate measurements of their excitability. We have previously shown that mouse motoneurons have shorter time constants than cats (Manuel et al., 2009). Mouse FF motoneurons have an average time constant of 2.1±0.2 ms, FR motoneurons 2.9±0.9 ms, while S motoneurons have a time constant of 4.0±0.7 ms (unpublished data from Martínez-Silva et al., 2018). Based on our present results, which show that a DCC frequency corresponding to at least 15 cycles per time constant is required to measure the excitability of the cell, FF motoneurons should be recorded with a DCC at at least 7 kHz, while S motoneurons can accommodate DCC frequencies as low as 3.75 kHz. Because of their size, FF motoneurons are also the cells that require the most current to fire. The impedance of the electrode is often highly non-linear, and both the resistance and the time constant of the electrode have a tendency to increase with the amount of injected current. Consequently, It is often difficult to record the firing of these cells at high DCC rates. Instead, it would be tempting, particularly in these cells, to lower the DCC rate to obtain proper settling of the electrode's IR drop, but, as we demonstrate here, doing so would lead to an overestimation of the cell's firing and excitability parameters. Moreover, in a mouse model of Amyotrophic Lateral Sclerosis, we have shown that the largest motoneu-

rons become incapable of firing repetitively in response to a slow ramp of current (Martínez-Silva et al., 2018). Given the membrane time constants of these cells, it was essential to perform these recordings at high DCC rates (all of our recordings were performed in DCC at 7–9 kHz), since lower DCC rates have the potential to distort the firing of these cells, and even mistakenly transform a non-repetitively-firing motoneuron into a repetitively-firing motoneuron (Jensen et al., 2020).

# 4 Conclusions

In conclusion, the effects of inappropriate DCC switching rates on the apparent conductance of the cells is well known. However, the effect on the firing characteristics of the neurons are not often discussed. We show here that choosing a sub-optimal DCC rate may dramatically distort parameters that are classically used to define the "excitability" of neurons: lower current onset, lower current offset, higher firing frequencies, higher F-I gains, and even the appearance of an artifactual "secondary range" of firing. Low DCC rates can therefore lead to a misrepresentation of neuronal excitability.

# 5 Methods

## 5.1 Animals

All procedures were approved by the Paris Descartes University ethics committee (CEEA34; authorization number 2018052100307589) and followed the European Directives (86/609/CEE and 2010-63-UE) and the French legislation on the protection of animals used for scientific purposes. Three C57BL/6 and four B6SJL male mice (weight 25–31 g; 27.9±2.3 g; N=7) were used in this study.

## 5.2 Experimental procedure

The surgical procedures have been described previously (Manuel et al., 2009; Manuel and Heckman, 2012). Briefly, atropine (0.20 mg/kg; Aguettant) and methylprednisolone (0.05 mg; Solu-Medrol; Pfizer) were given subcutaneously at the onset of experiment, to prevent salivation and oedema, respectively. Fifteen minutes later, anaesthesia was induced with an intraperitoneal injection of sodium pentobarbitone (70 mg/kg; Pentobarbital; Sanofi-Aventis). A tracheotomy was performed, and the mouse was artificially ventilated with pure oxygen (SAR-830/AP ventilator; CWE). The end tidal CO2 level was maintained around 4% (MicroCapstar; CWE). The heart rate was monitored (CT-1000; CWE), and the central temperature was kept at 37°C using an infrared heating lamp and an electric blanket. A catheter was introduced in the external jugular vein, allowing us to supplement the anaesthesia whenever necessary (usually every 20–30 min) by intravenous injections (sodium pentobarbitone, 6 mg/kg). The adequacy of anaesthesia was assessed on lack of noxious reflexes and on the stability of the heart rate (usually 400–500 bpm) and end-tidal PCO2. A slow intravenous infusion (50 µL/h) of a 4% glucose solution containing NaHCO3 (1%) and gelatine (14%; Plasmagel; Roger Bellon) helped maintain the physiological parameters. The animal was paralyzed after the surgery with atracurium besylate (Kalceks; initial bolus was 0.1 mg, followed by a continuous infusion 0.01 mg/h). Additional doses of anaesthetics were then provided at the same frequency as before the paralysis, and adequacy of anaesthesia was assessed on the stability of the heart rate and of PCO2. The vertebral column was immobilized with two pairs of horizontal bars (Cunningham Spinal Adaptor; Stoelting) applied on the Th12 and L2 vertebral bodies, and the L3–L4 spinal segments were exposed by a laminectomy at the Th13–L1 level. The Triceps Surae nerve (containing the branches innervating the Medial Gastrocnemius, the Lateral Gastrocnemius and the Soleus) was dissected and placed on a bipolar electrode for stimulation. All other branches of the sciatic

nerve were cut. The tissues in the hindlimb and the spinal cord were covered with pools of mineral oil. At the end of the experiments, animals were killed with a lethal intravenous injection of pentobarbitone (200 mg/kg).

## 5.3 Electrophysiological recordings

The motoneurons were impaled with micro-pipettes (tip diameter, 1.0–1.5 μm) filled with either 3 M KCl or 3 M K-Acetate (resistance 23.1±5.9 MΩ [16.0–33.0 MΩ], N=13). Recordings were performed using an Axoclamp 2B amplifier (Molecular Devices) connected to a Power1401 interface and using the Spike2 software (CED). The current ($I_m$) and voltage output ($10V_m$) of the amplifier were low-pass filtered at 10 kHz and sampled at 20 kHz. When recorded, the continuous output $I_1$ and $V_1$, and the DCC monitor output were sampled at 100 kHz. After impalement, identification of motoneurons rested on the observation of antidromic action potentials in response to the electrical stimulation of their axon in the triceps nerve. All care was taken to compensate for the microelectrode resistance and capacitance. No bias current was used to maintain the resting membrane potential. All cells kept for anaysis had a resting membrane potential more hyperpolarized than −50 mV and an overshooting antidromic spike. As fully described previously (Manuel et al., 2009), the input resistance was measured using the peak response of a series of small-amplitude square current pulses (−3 to +3 nA, 500 ms) recorded in DCC mode (8 kHz). The membrane time constant was measured on the relaxation of the membrane potential after injection of small hyperpolarizing current pulses (−5 nA, 1 ms), recorded in Bridge mode. Slow triangular ramps of current were injected in DCC mode (switching rates as described in the text). A recovery period of at least 30s was left in between each repetition. Using an offline automated script, the timing of each spike was recorded along with the current intensity at that time to construct the F-I curve. At switching rates <3 kHz, the DCC voltage trace was often too distorted to identify spikes reliably. In these cases, the continuous voltage trace

was carefully scanned manually to identify spikes. The onset current was defined as the value of the injected current at which the first action potential was generated one the ascending phase of the ramp. The offset current was the current intensity corresponding to the last action potential on the descending phase of the ramp. The F-I gain was measured as the slope of the F-I relationship in the most linear part of the ascending phase of the ramp ("primary range"). The voltage threshold was measured at the point when the slope of the membrane voltage crosses 10 mV/s (Sekerli et al., 2004) just prior to the first spike of the ascending phase of the ramp.

## 5.4 Numerical simulations

Numerical simulations were conducted using the Brian2 simulator (v.2.4.1) in Python v.3.8 and using the SciPy ecosystem (v.1.5.0; Virtanen et al., 2020).

For investigating membrane potential ripples (Figure 2), both the cell and the electrodes are modeled as passive RC circuits with equations:

$$\begin{aligned} C * \frac{dV}{dt} &= G * (V_0 - V) + I_{inj} \\ C &= G * \tau \end{aligned} \tag{1}$$

For the cell, $G_{in}$ was set to 0.2 μS and $\tau_m$=5 ms. To model the IR drop through the electrode, parameters were chosen so that the electrode was 200× faster than the membrane time constant ($\tau_e$=$\tau_m$/200=25 μs). The equation above was solved with $G_e$=1 μS. Although not quite realistic, this value was chosen so that the response of the electrode would not completely dominate the graphs in Figure 2. Note however that the value of the resistance of the electrode is only relevant at high DCC rates, when the IR drop through the electrode does not have time to vanish by sampling time (Figure 2). At lower switching rates, the resistance of the electrode is irrelevant since its contribution has fully dropped to zero at the end of the DCC period.

For investigation of the effect of the DCC rate on firing, we used as simple integrate-

and-fire model with a passive leak conductance and an after-hyperpolarization (AHP) current (Meunier and Borejsza, 2005; Manuel et al., 2006). The membrane potential ($V_m$) is governed by the equations:

$$\begin{aligned} C * \frac{dV_m}{dt} &= G_{in} * (V_r - V_m) + I_{AHP} + I_{inj} + \sigma\xi \\ C &= G_{in} * \tau_m \\ I_{AHP} &= \bar{g}_{AHP} * z * (E_k - V_m) \\ \frac{dz}{dt} &= \frac{-z}{\tau_{AHP}} \end{aligned} \tag{2}$$

$G_{in}$ is the input conductance of the cell (we used the values 0.2 μS, 0.4 μS, and 0.67 μS for S, FR and FF motoneurons, respectively, see text). $\tau_m$ is the membrane time constant (varied between 2 and 5 ms, see text). $V_r$ is the resting membrane potential (0 mV). $\sigma\xi$ is a noise term. $I_{AHP}$ is the AHP current. $\bar{g}_{AHP}$ is the maximum conductance of the AHP (2 μS), $E_k$ is the reversal potential of the AHP (-5 mV). $z$ is the fraction of the AHP conductance open at any point in time, and $\tau_{AHP}$ is the relaxation time constant of the AHP (10 ms). For simplicity, the dynamic of the AHP during the spike is not modeled, and instead, the parameter $z$ is incremented instantaneously at each spike (elicited when $V > V_{thr}$, $V_{thr}$=10 mV) according to $z_{after} = (1-\alpha) * z_{before} + \alpha$, where $\alpha$ is the fraction of the AHP recruited by a single spike ($\alpha$=0.25) (Meunier and Borejsza, 2005), $z_{before}$ is the value of $z$ just prior to the spike and $z_{after}$ the value of $z$ just after the spike. $I_{inj}$ is the current injected by the amplifier in bridge mode. In DCC mode, this current is chopped and scaled with a duty cycle of 1/3. DCC rates range from 1 to 8 kHz.

## 5.5 Code availability

All figures were drawn using matplotlib v.3.2.2 (Hunter, 2007). The code for analysis and production of figures is available at https://doi.org/10.5281/zenodo.4139701.

## Competing interests

The author declares no conflict of interests.

## Grant information

This work was financed by NIH NINDS R01 NS110953.

## Acknowledgements

The author wishes to thank Drs. Daniel Zytnicki, Rob Brownstone, and Marco Beato for their valuable comments and discussions. This work has benefited from the support and expertise of the animal facility and microscopy platform of BioMedTech Facilities at Université de Paris (INSERM US36/UMS2009).

## References

Agrawal N, Hamam BN, Magistretti J, Alonso A & Ragsdale DS (2001). Persistent sodium channel activity mediates subthreshold membrane potential oscillations and low-threshold spikes in rat entorhinal cortex layer V neurons. *Neuroscience* **102**, 53–64.

Axon Instruments I (2003). Axoclamp-2B, Microelectrode Clamp, Theory and Operation.

Azouz R & Gray CM (2000). Dynamic spike threshold reveals a mechanism for synaptic coincidence detection in cortical neurons in vivo. *Proceedings of the National Academy of Sciences of the United States of America* **97**, 8110–8115.

Brennecke R & Lindemann B (1971). A chopped-current clamp for current injection and recording of membrane polarization with single electrodes of changing resistance. *T-I-T-J Life Sci.* **1**, 53–58.

Brette R & Destexhe A (2012). Intracellular recording In *Handbook of Neural Activity Measurement*. Cambridge University Press.

Delestrée N, Manuel M, Iglesias C, Elbasiouny SM, Heckman CJ & Zytnicki D (2014). Adult spinal motoneurones are not hyperexcitable in a mouse model of inherited amyotrophic lateral sclerosis. *The Journal of physiology* **592**, 1687–703.

Finkel AS & Redman S (1984). Theory and operation of a single microelectrode voltage clamp. *Journal of Neuroscience Methods* **11**, 101–127.

Gustafsson B & Pinter MJ (1984). Relations among passive electrical properties of lumbar alpha-motoneurones of the cat. *The Journal of physiology* **356**, 401–31.

Hunter JD (2007). Matplotlib: A 2d graphics environment. *Computing in Science & Engineering* **9**, 90–95.

Iglesias C, Meunier C, Manuel M, Timofeeva Y, Delestrée N & Zytnicki D (2011). Mixed mode oscillations in mouse spinal motoneurons arise from a low excitability state. *The Journal of neuroscience : the official journal of the Society for Neuroscience* **31**, 5829–40.

Jensen DB, Kadlecova M, Allodi I & Meehan CF (2020). Spinal motoneurones are intrinsically more responsive in the adult G93A SOD1 mouse model of Amyotrophic Lateral Sclerosis. *The Journal of Physiology* **n/a** _eprint: https://physoc.onlinelibrary.wiley.com/doi/pdf/10.1113/JP280097.

Kuo JJ, Lee RH, Zhang L & Heckman CJ (2006). Essential role of the persistent sodium current in spike initiation during slowly rising inputs in mouse spinal neurones. *The Journal of Physiology* **574**, 819–834.

Mainen Z & Sejnowski T (1995). Reliability of spike timing in neocortical neurons. *Science* **268**, 1503–1506.

Manuel M & Heckman CJ (2012). Simultaneous intracellular recording of a lumbar motoneuron and the force produced by its motor unit in the adult mouse in vivo. *Journal of visualized experiments : JoVE* **70**, e4312.

Manuel M, Iglesias C, Donnet M, Leroy F, Heckman CJ & Zytnicki D (2009). Fast kinetics, high-frequency oscillations, and subprimary firing range in adult mouse spinal motoneurons. *The Journal of neuroscience* **29**, 11246–11256.

Manuel M, Meunier C, Donnet M & Zytnicki D (2006). The afterhyperpolarization conductance exerts the same control over the gain and variability of motoneurone firing in anaesthetized cats. *The Journal of physiology* **576**, 873–886.

Martínez-Silva MdL, Imhoff-Manuel RD, Sharma A, Heckman C, Shneider NA, Roselli F, Zytnicki D & Manuel M (2018). Hypoexcitability precedes denervation in the large fast-contracting motor units in two unrelated mouse models of ALS. *eLife* **7**, e30955.

Meunier C & Borejsza K (2005). How membrane properties shape the discharge of motoneurons: a detailed analytical study. *Neural computation* **17**, 2383–2420.

Sekerli M, Del Negro CA, Lee RH & Butera RJ (2004). Estimating action potential thresholds from neuronal time-series: new metrics and evaluation of methodologies. *IEEE transactions on bio-medical engineering* **51**, 1665–1672.

Virtanen P, Gommers R, Oliphant TE, Haberland M, Reddy T, Cournapeau D, Burovski E, Peterson P, Weckesser W, Bright J, van der Walt SJ, Brett M, Wilson J, Jarrod Millman K, Mayorov N, Nelson ARJ, Jones E, Kern R, Larson E, Carey C, Polat İ,

Feng Y, Moore EW, Vand erPlas J, Laxalde D, Perktold J, Cimrman R, Henriksen I, Quintero EA, Harris CR, Archibald AM, Ribeiro AH, Pedregosa F, van Mulbregt P & Contributors S (2020). SciPy 1.0: Fundamental Algorithms for Scientific Computing in Python. *Nature Methods* **17**, 261–272.